HA/ZrO_2 Coating on CoCr Alloy Using Flame Thermal Spray

Juliano, Hans
Mechanical Engineering Department, Faculty of Engineering, Brawijaya University

Gapsari, Femiana
Mechanical Engineering Department, Faculty of Engineering, Brawijaya University

Izzuddin, Hubby
Research Center for Advanced Materials, National Research and Innovation Agency

Sudiro, Toto
Research Center for Advanced Materials, National Research and Innovation Agency

他

HA/ZrO₂ Coating on CoCr Alloy Using Flame Thermal Spray

Hans Juliano[1], Femiana Gapsari[1,*], Hubby Izzuddin[2], Toto Sudiro[2],
Krisna Yuarno Phatama[3], William Putera Sukmajaya[3], Zuliantoni[1,4],
Thesya Marlia Putri[1], Abdul M Sulaiman[1]

[1] Mechanical Engineering Department, Faculty of Engineering, Brawijaya University, Indonesia.

[2] Research Center for Advanced Materials, National Research and Innovation Agency, Indonesia

[3] Orthopaedic and Traumatology Department, Faculty of Medicine, Brawijaya University, Saiful Anwar General Hospital Malang, Indonesia.

[4] Mechanical Engineering Department, Faculty of Engineering, Bengkulu University, Indonesia.

* E-mail: memi_kencrut@ub.ac.id

Abstract: CoCr alloy is mostly used as biomaterial implant. However, it still has several weaknesses. Therefore, it is necessary to modify the surface to improve its biocompability. This research is a preliminary study on CoCr coated with Hydroxyapatite (HA)/Zirconium Dioxide (ZrO₂) using Thermal Flame Spray method. 5 % - 20 % ZrO₂ was mixed with HA. Besides improving the biocompatibility, ZrO₂ is believed to be able to enhance the antibacterial properties. Characterization test was performed using FE-SEM. The coating was analyzed for corrosion rate, surface roughness and antibacterial activity. Adding ZrO₂ to HA has been proven to be able to improve corrosion rate. Combination of 80HA-20ZrO₂ is the most effective bioceramic mixture, producing lowest corrosion rate of 0.213 mm/year in HBSS media. This is due to the increased reactivity value and better passivation reaction than CoCr without coating. Antibacterial activity test revealed that the coating could form inhibitory area around the sample meaning that the coating can provide bacterial resistance for the implant.

Keywords: biomaterial; CoCr alloys; hydroxyapatite; zirconium dioxide; thermal flame spray, corrosion rate

1. Introduction

Biomaterial should have resistance to corrosion, fatigue, wear, abrasion, and low surface hardness [1]. Several types of metal meet the requirements to be used as biomaterial, including SUS 316L, Ti CP Grade 1-4, and CoCr [2,3]. Co-Cr alloy is widely used to make prostheses such as orthopedic devices, dental and cardiovascular implants [4–6]. However, there are still some problems regarding the use of the alloy, such as wear-included osteolysis, modulus differences between bone and implants, metal ions release due to bio tribo corrosion [7]. The alloy contains more than 20 % of Cr mass which is able to improve the corrosion resistance by forming a passive layer which is mostly contained of oxide [8]. Co-Cr alloy has high compatibility and good mechanical characteristics. However, it has low bioactivity that causes weak bone bonds [9,10]. To improve the bioactivity, chemical modification process is needed on the alloy surface [11].

Interaction of an implant with living tissue is indicated by its bioactivity characteristic. The characteristic is important to observe and should be avoided because it is prone to bacterial infection [12]. Infection is the most severe form of complication and destroys biomaterial function [13]. Improvement of biocompatibility of metallic-orthopedic prothesis can be done by covering the prothesis using other materials with better properties such as bio ceramic coatings [2], e.g., inert ceramics to cover metal prothesis. The term inert is used for materials in the body which do not cause poisoning, thus avoiding infection. In the body, these materials stimulate tissue production to cover and protect the prothesis [14]. Several types of bio inert ceramics that can be used are titanium dioxide (TiO2), zinc oxide (ZnO), hydroxyapatite (HA) and zirconium dioxide (ZrO₂) [15,16].

HA coating is considered to be an appropriate approach to solve the problem [17]. HA acts as a barrier against the release of metal ions from the substrate in biological environment [18]. HA has chemical and biological material which is similar to human bone. The result of HA coating can improve the growth of bone cells to increase the interaction between the implant and the surrounding tissue (this is called osseointegrassion) [19]. However, HA coating

degrades over time due to its brittle nature and lack of sufficient mechanical and physical properties to withstand long-term performance (e.g., lower fracture toughness and lower tensile strength) [20]. Compared to several other coatings, ZrO_2 can be a viable candidate for the purpose because of its biocompatibility, chemical inertness, mechanical strength, thermal stability, wear and corrosion resistance, also the value of Young's modulus which is almost the same as stainless steel [21]. ZrO_2 has hydrophilic properties that are able to protect the substrate from the attachment of bacteria to its surface to provide protection against bacteria [22]. Interfacial corrosion of the substrate layer may occur and result in poor mechanical strength and coating adhesion [23,24]. Therefore, selecting coating method is very important to get coating that can improve the biocompatibility. Thermal spray can be one of the good choices.

Several common methods used in metal coating are APS (arc plasma spray), HVOF (high velocity oxygen fuel) and flame spray. Flame spray is used more because it is more economical [25]. However, flame spray coating on Co-Cr causes porosity [26]. This is caused by the lack of fusion between the sprayed particles and the produced gas expansion during the spraying [27,28]. Besides that, deposition process at high temperatures, oxidized atmospheric environment and a high cooling rate also cause porosity [29,30]. Adding ZrO_2 to HA is conducted to get lower porosity. In this study, the Co-Cr alloy material was coated with a mixture of HA-ZrO_2 using the flame spray coating method with different contents. The effect of HA/ZrO_2 particles on corrosion rate in Co-Cr coating was studied using electrochemical test. The coating formed was characterized using SEM and other testing.

2. Material and Method

2.1 Substrate Preparation

The CoCr substrate (ASTM F75) was provided by Suzhou Chuan Mao Metal Material, China. It was in the form of cylinder with diameter of 8 mm and length of 8 mm. Hole making was done by drilling EDM drill with a size of 2 mm on central part of the substrate. The composition of the sample was 0.10 Si, 0.10 Mn, 29.7 Cr, 0.2 Ni 5.85 Mo, and 0.025 Fe (wt. %).

2.2 Preparation of Coating Powder

The coating powder used was the mixture of HA/ZrO_2 with variations shown in Table 1. The sizes of hydroxyapatite were 30 - 80 μm. Zirconium Dioxide used in the study was obtained from Xi'an Benher Biotech Co, Ltd. with particle size average of 0.7 μm. The Composition variations of coating material are shown in detailed in Table 1. The composition variations were 95% HA/5% ZrO_2 (I), 90% HA/10% ZrO_2 (II), and 80% HA/20% ZrO_2 (III). Powder mixing was done by weighing each type of powder and putting the mixture in a jar. Next, it was shaken for about 5 minutes.

Table 1. The composition of coating variable

Code	HA (%wt)	ZrO_2 (%wt)
I	95	5
II	90	10
III	80	20

2.3 The process of Thermal Flame Spray

The surface of CoCr was roughened by applying grit blasting test process using aluminum oxide (Al_2O_3), then cleaned using ultrasonic cleaner with acetone solution for 2 minutes. The coating process used a Metallization MK74-C Flame Spray Gun. 304SS wire with a diameter of 1.5 mm was used to clamp the sample and acted as a shaft to rotate the sample. The specimen clamping wire was rotated at a speed of 60 rpm using a modified electric drill. The spraying was performed with fuel flow rate of 4 LPM, oxygen flowrate of 6 LPM, air pressure of 2 bar, spraying distance of 75 mm and spraying angle of 90°.

2.4 SEM Morphology

The characterization process is carried out by making cross-section cut of the specimen that has been mounted on resin, cut and polished to a mirror finish. Then, FE-SEM-EDS Jeol JIB-4610F was used. Next, Image J software was used to calculate porosity value. The average values of the total surface area of the sample and the total area of porosity were calculated. The coating thickness test was analyzed with the help of Image J software. Data of thickness were collected from 10 different areas to get the average value. The characterization of the element distribution was carried out using Oxford Instruments X-Max EDS with AZtecLive Spectrum Analysis software.

2.5 Surface Roughness Tester

The test was performed using Mitutoyo SJ 201 tool. The specimen was placed on V-Block. Stylus surface roughness tested was paired with height gauge so that the tip of stylus touched the specimen surface.

2.6 Corrosion Test

100 ml Hank's balance salt solution (HBSS) was prepared and then heated until it reached body temperature of 34°C-36°C. Then, corrosion rate testing tool of Autolab PGSTAT 204N and NOVA 1.11 were prepared. The test was done with scan rate of 0.005 v/s at the open circuit at range of ± 2.5 V. The test used 3-electrode principle with the coated CoCr specimen as the working electrode, Pt as the reference electrode, and Ag/AgCl KCl 3M reference electrode.

2.7 Antibacterial Test

Antibacterial test was conducted to know the antibacterial properties of the coating. The process was done by making bacterial suspension of one inoculating loop. The rejuvenated bacteria were put into test tube containing physiological NaCl solution (Otsuka), then

incubated for 24 hours at temperature of 37° C. The turbidity was made equivalent to 0.5 McFarland. The suspension turbidity was compared by placing a standard McFarland tube and a bacterial culture tube in front of black-lined white paper. Furthermore, a swab of the test bacterial suspension which had been equalized with a standard solution of 0.5 McFarland was streaked on the entire surface of the NA medium in a petri dish. Three wells were made on the NA medium which was inoculated with the test bacteria using tip holes. On each petri dish and in each hole, 150 μL of test solution was added. The petri dish was incubated for 24 hours at temperature of 37° C. After the incubation was completed, the inhibition zone was observed and measured using a ruler. The inhibitory strength was grouped based on its diameter as in Table 2.

Table 2. Classification of clear zone response

Inhibiting response	Diameter of clear zones
No Response	< 5 mm
Medium	5 – 10 mm
Strong	10 – 20 mm
Very Strong	> 20 mm

3. Results

3.1 The Analysis of Coating Porosity

Morphology observation in Figure 1 (a-c) shows that the three coatings are not homogeneous and look cracked. The middle part in each figure (Figure 1a – c) shows the results of segmentation of porosity color and the background color. The lower part in each figure (1a – c) displays the result of porosity analysis process.
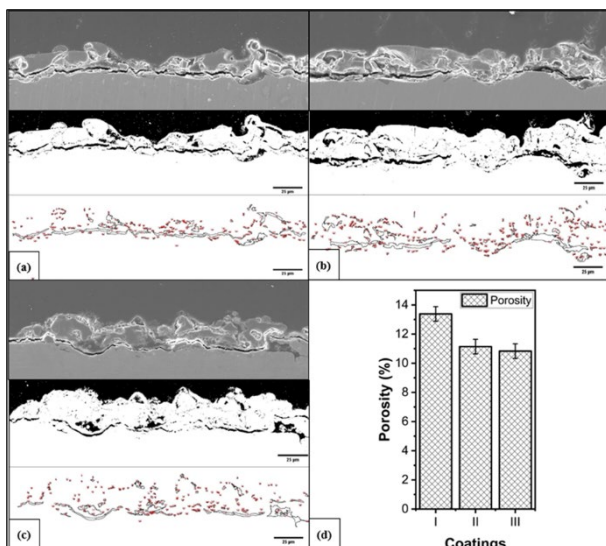

Fig. 1: Porosity analysis using particle analyze feature in ImageJ software (a) I (b) II (c) III and (d) coating porosity

Figure 1 conveys that there are 210 porosity spots obtained from the porosity analysis on Coating I. Figure (b) shows that there are 241 porosity spots derived from

porosity analysis on Coating II. Displayed in Figure (c), there are 196 porosity spots gained from porosity analysis on Coating III. The results of porosity analysis can be seen in Figure 1 (d). It shows that the highest percentage (13.38%) is found in coating I, while the coating III has the lowest porosity (10.83%).

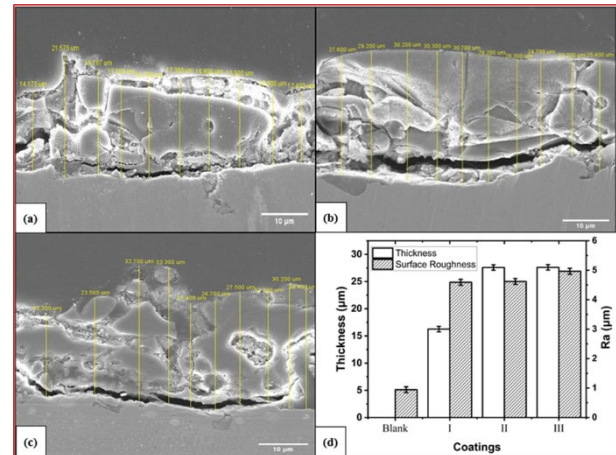### 3.2 The Surface Roughness Test and Coating Thickness Analysis

Fig. 2: Coating thickness measurement on cross section cut: (a) I, (b) II, (c) III (d) thickness and coating surface roughness

Figure 2 (a-c) details the result of coating thickness measurement on cross section cut on Coating I, II, and III. Yellow line in Figure 2a is the thickness of Coating I varying between 12.400 to 21.58 μm. Figure 2b shows that thickness of Coating II is higher ranging from 25.400 to 30.200 μm. Figure 2c is Coating III with thickness ranging from 20.200 to 33.300 μm. Comparison of average thickness of Coating I, II, and III can be seen in Figure 2d. It reveals that the coating has the lowest average thickness of 16.26 μm. Coating II has much higher average thickness than coating I, but lower than the average thickness of Coating III (27.61 μm).

The result of roughness test can be seen in Figure 2d which shows that Composition III has the highest roughness (Ra) of 4.963 μm. The lowest roughness of 4.591 μm is produced by Composition I. In uncoated CoCr, the average roughness value is 0.944 μm.

3.3 Observation of Elements Distribution

Figure 3 is the analysis of elements distribution in Coating 1, II, and III. The most even element distribution is in specimen code III.
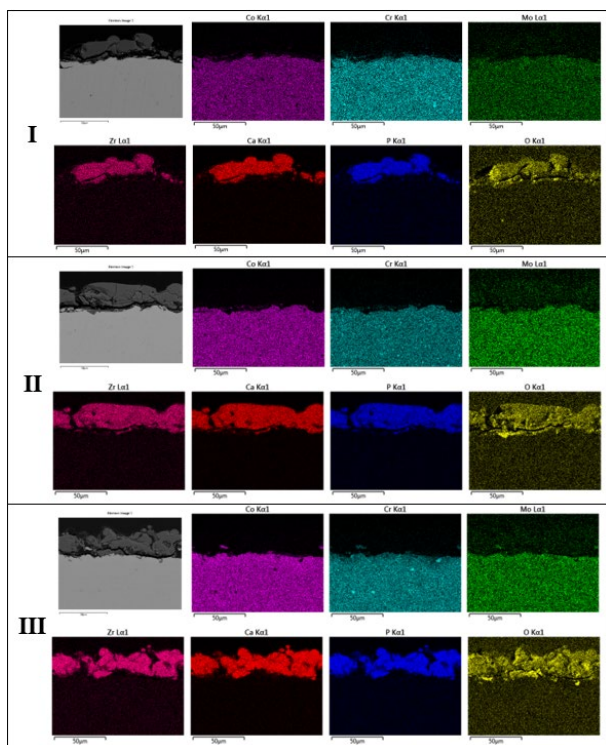
Fig. 3: Porosity analysis using particle analyze feature in ImageJ software (a) I (b) II (c) III and (d) coating porosity

3.4 Electrochemical Test

The curves of potentiodynamic polarization can be seen in Figure 4. The corrosion parameters are shown in Table 3.
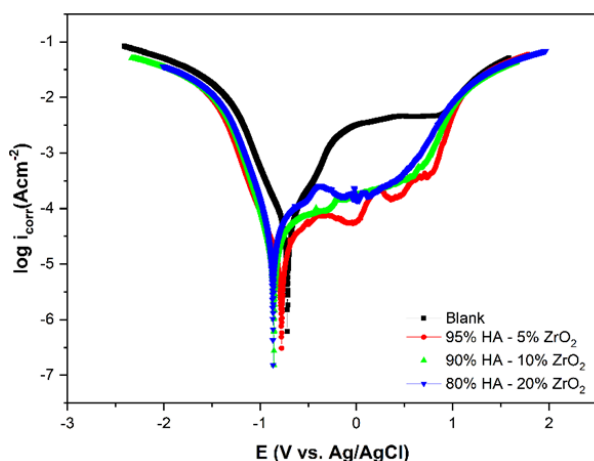

Fig. 4: The curves of potentiodynamic polarization in HBSS medium

Table 3. Corrosion parameters using Tafel Extrapolation method

Coatings	β_a (V/dec)	$-\beta_c$ (V/dec)	E_{corr}, (V)	i_{corr} (A/cm²)	Corrosion Rate (mm/year)
Blank	0.09	0.13	-0.72	2.21×10^{-5}	1.82
I	0.1	0.06	-0.78	4.11×10^{-6}	0.34
II	0.03	0.05	-0.86	3.36×10^{-6}	0.28
III	0.02	0.02	-0.87	2.59×10^{-6}	0.21

Table 3 details that the lowest corrosion rate (0.21 mm/year) is found in the coating with composition of mixture III. The highest corrosion rate (0.34 mm/year) is in the coating with composition of mixture I. As a comparison, corrosion test was conducted on blank coating with corrosion rate of 1.82 mm/year.

3.5 Antibacterial Activity

The result of inhibition zone diameter is shown in Figure 5 (c) dan (d). It is revealed that the coating has antibacterial properties on both types of bacteria. Inhibition zone produced is getting bigger along with the ZrO_2 addition to the coating. Thus, it can be assumed that there is a directly proportional relationship between the addition of ZrO_2 and the result of inhibition zone. Seen from the test result, the inhibition zone diameter is larger in gram negative bacteria than in gram positive bacteria.
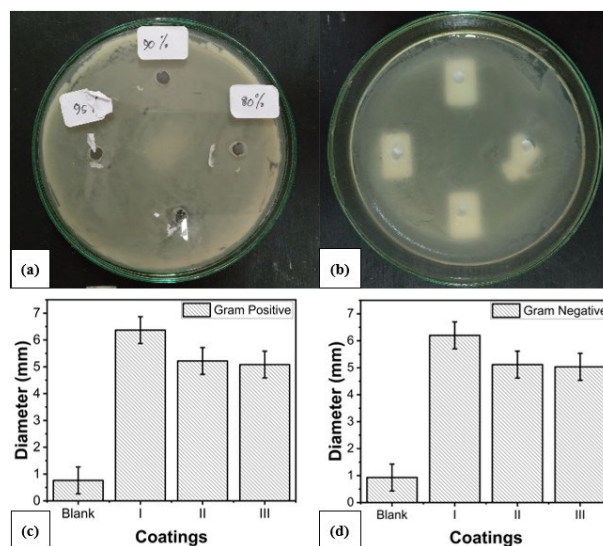

Fig. 5: Antibacterial test on coating (a) gram positive bacteria to make it sterile (b) gram negative bacteria to make it sterile (c) the results of antibacterial test on gram positive bacteria (d) The results of antibacterial test on gram negative bacteria.

4. Discussion

The result of porosity test of each coating is displayed in Figure 4. Porosity value is getting lower along with the addition of ZrO_2 in the coating mixture. This happens because The speed of the particles will increase during the spraying if the particle size is smaller [31]. When the particle speed is getting higher during the spraying, the coating quality will be better because it produces coating with minimum oxidation and porosity [32]. Porosity is necessary because it provides a specific area for calcium phosphate nucleation, increases bond strength, and reduces surface failure [33]. The porosity is higher at lower spraying energies, where the semi-liquid particles are less deformed. At higher spray energies, the liquid material with high diffusivity will fill the asperities and gaps of the previously deposited layer, leading to lower porosity [34].

Porosity slightly increases along with the addition of ZrO$_2$. Therefore, it can be said that HA is the cause of porosity deviation in the composite. Furthermore, it has been analyzed that the porosity can be increased after the addition of HA to the substrate due to difference in the coefficient of thermal expansion between the substrate and HA during sintering [35], although the presence of a phase with lower ionic conductivity than HA such as ZrO$_2$ as a reinforcement indicates that corrosion resistance will increase [36]. However, the presence of various elements in the sample can cause galvanic effect which causes corrosion resistance degrades. Curran et. al. [37] mentioned that 5% ZrO$_2$ additive was applied to the HA grain boundaries effectively, reducing porosity.

The roughness test revealed that there was difference in surface roughness among the three coating although the spraying parameters were the same. The characteristics of the powder used on each coating were different. Adding ZrO$_2$ into the mixture increased the surface roughness of the coating. This is seen from the value of Ra (4.963 μm) at the highest composition of 80HA-20ZrO$_2$ than the composition on other coatings. Visible microcracks were due to the combination of brittleness and plasticity of the composite coating [38]. The surface roughness of the substrate caused the atoms to be tilted and exposed diagonally to the surface, thereby increasing the porosity of the coating [39]. Surface roughness has important role in implant making. Higher surface roughness increases the contact between the bone and the implant, but only over a very narrow range of 1-1.5 μm [40]. Several studies show that increasing surface roughness increases cell attachment, proliferation, and differentiation [41]. The other study state that surface roughness reduces the cell function and bond formation [42]. The change in surface roughness in 10 nm - 10 μm has a little effect on the interfacial mechanical characteristic, but significant effect on biocompatibility because the range of dimension is at the same level of magnitude with the cell size and biological macromolecules size. As the surface roughness increases, the adhesion and osteoblast proliferation ability increases, which is beneficial for the attachment and osteoblast proliferation when the surface roughness is high (Ra >1.5 μm) [43].

From the analysis of coating element distribution, it is confirmed that Specimen I has the lowest Zr content, followed by Specimen II and Specimen III. The thickness of Zr color represents the number of elements contained. This is in line with the composition of mixture where the Specimen III has composition of 20 % ZrO$_2$ which is more than the Specimen I and III that only have 10 % and 5 % ZrO$_2$. The elements analysis revealed that all coating had even mixture of ZrO$_2$ and HA. The coating looks homogeneous with even distribution on overall surface. The difference between the coating and the substrate is clearly visible. Bioactivity test in Hank's solution showed that the HA powder was able to induce nucleation and deposition of Ca and P with HA typical morphology [44].

SEM-EDS results showed that HA/ZrO$_2$ after immersion in Hank's solution underwent a typical structural change in the process of apatite formation. The first change is the growth of Ca-rich layer. The second structural change is based on the interaction of the Ca-rich surface with negative ions such as phosphate to form a Ca-poor layer. Then, the layer crystallized and formed apatite. This proses causes the change in ratio of Ca/P due to ions exchange [45]. EDS analysis identified that zirconium dioxide obtained consisted of Zr and O. Zr was uniformly distributed with obvious granularity on the coating surface, which was attributed to ultrasound during electrodeposition leading to homogeneous distribution of ZrO$_2$ in the matrix. O was evenly distributed on the coating surface. Uniform distribution of elements leads to the formation of a compact layer and consequently improves mechanical properties [46].

From the testing, it was known that there was an increase in the coating thickness along with the addition of ZrO$_2$ into the coating mixture. ZrO$_2$ has smaller size of particle (600 μm) than HA (30 μm). Generally, the surface roughness increases with thickness due to the presence of large channels remaining from a single splash in the coating [47]. As the particle size decreases, the coating thickness will increase, because there is a decrease in the indentation force as the particle size decreases [48]. Higher thickness usually parallels higher surface roughness. These two factors support each other and oppose the properties of the phosphate-containing coating. Thus, sample of 80HA – 20ZrO$_2$ provides the highest corrosion resistance.

Implant corrosion test in HBSS solution revealed the results that all coatings are able to provide better corrosion resistance than the uncoated CoCr. Adding ZrO$_2$ into coating composition can improve the implant corrosion resistance. This is known from Figure 4 and Table 3, explaining that coating with Composition I has Tafel plot which tends to shift to active direction and the lowest corrosion rate than others with coating composition. ZrO$_2$ forms thin ion layer that is able to protect from corrosion. The corrosive substances cannot penetrate the oxide layer on ZrO$_2$ to cause corrosion [22]. Corrosion resistance gets better with the improvement of biocompatibility of an implant [49]. Adding ZrO$_2$ into coating can suppress corrosion rate compared to coating that uses less ZrO$_2$. The lower HA or the higher ZrO2 in HA/ZrO$_2$ mixture, the more active the value of Ecorr. Using the Tafel extrapolation method, the anodic Tafel slope (βa), cathodic Tafel slope (βb), corrosion current (icorr), corrosion potential (Ecorr) and corrosion rate are summarized in Table 3. As it is known, icorr can represent the corrosion rate of metal surfaces [50]. The corrosion current and corrosion rate of all HA/ZrO$_2$ layers are lower than that of the blank substrate. This result indicates that all HA/ZrO$_2$ coating is effective in preventing penetration of electrolyte ions on the surface of metal substrate [51]. Corrosion rate increases along with the increase of coating

porosity. Corrosion resistance is affected by crystallinity, purity, residual stress and ion substitution in the layered structure and apatite lattice [52]. The increased corrosion rate in the HA rich layer, i.e. (HA-ZrO$_2$ coated sample) may be due to (a) higher roughness, (b) presence of a larger porosity area fraction and (c) higher HA content in the coating [53]. Sasaki and Burstein [54] state that the potential of steel pitting decreases because surface roughness increases. This result is supported by another study [55], which shows that a greater roughness corresponds to a lower hole potential (the potential at which metastable holes begin to form on the surface).

After antibacterial activity test on HA-ZrO$_2$ coating, it was found that the coating could form inhibitory area around the sample. Bacterial inhibitory area in all samples with coating has diameter of > 5 mm which means it has moderate bacterial resistance response [56]. The size of the inhibition zone formed varies depending on the anti-bacterial ability of the coating against each type of test bacteria. This indicates that there are bioactive compounds in the coating which are able to inhibit the growth of test bacteria [57]. The biggest antibacterial activity is shown by coating on Specimen I, while the lowest antibacterial activity is found in coating on Specimen III, on both gram-positive and gram-negative bacteria.

5. Conclusion

Adding HA-ZrO$_2$ bio ceramic into the CoCr alloy coating using flame thermal spray method has been proven to improve the corrosion resistance of the material in HBSS corrosive media. Addition of 80 % HA and 20 % ZrO$_2$ provides the lowest corrosion rate which is 0.213 mm/year. The coating on substrate is able to prevent electrolyte ions or electrons from entering the substrate surface. The coating with varied composition of bio ceramic produced varied thickness, porosity, and roughness although conducted with the same spraying parameter. This was due to different composition that changed the characteristics of coating powder, thereby causing different coating. The best composition is the combination of 80 % HA – 20 % ZrO$_2$ because it produced the lowest value of porosity and corrosion rate in HBSS media. However, this result cannot be applied in wider range of nanoparticles and additives. It is expected that the basic understanding gained in this work will start further exploration efforts to find new composite materials in the manufacture of hydroxyapatite composite layers.

References

1) J. Marzi, E. Brauchle, D.A. Carvajal Berrio, S. Lee Layland, and K. Schenke-Layland, "3.7 Raman spectroscopy," in: Comprehensive Biomaterials II, Elsevier, 2017: pp. 108–127. doi:10.1016/B978-0-12-803581-8.09323-1.

2) B. Raton, L. New, Y. Washington, J.B. Park, and J.D. Bronzino, "CRC PR E S S," n.d.

3) J. Triyono, R. Rahajeng, and E. Surojo, "Surface modification and hardness behavior of aisi 304 as an artificial hip joint using ammonia and scallop shell powder as a nitriding agent," Evergreen, 8 (2) 335–343 (2021). doi:10.5109/4480714.

4) P. Di, N.· Sanjiv, D. Dinender, and K. Singla Editors, "Adult Stem Cells Methods and Protocols Methods in Molecular Biology 1553," n.d. http://www.springer.com/series/7651.

5) M. Sharma, and M. Soni, "Transdisciplinary Research and Education Center for Green Technologies," 2020. http://hdl.handle.net/2324/4068615 Evergreen.7.

6) A.M. Rosli, A.S. Jamaludin, and M.N.M. Razali, "Recent study on hard to machine material - micromilling process," Evergreen, 8 (2) 445–453 (2021). doi:10.5109/4480727.

7) J. Fisher, X.Q. Hu, T.D. Stewart, S. Williams, J.L. Tipper, E. Ingham, M.H. Stone, C. Davies, P. Hatto, J. Bolton, M. Riley, and G. Berry, "A L S I N M E D I C I N E 1 5 (2 0 0 4) 2 2 5 ± 2 3 5 Wear of surface engineered metal-on-metal hip prostheses," n.d.

8) M. Takayukiinarushima, and M. Editors, "Springer Series in Biomaterials Science and Engineering 3 Advances in Metallic Biomaterials Tissues, Materials and Biological Reactions," n.d. http://www.springer.com/series/10955.

9) C. Liu, C. Matsunami, Y. Shirosaki, and T. Miyazaki, "Bioactive co-cr alloy for biomedical applications prepared by surface modification using self-assembled monolayers and poly-γ-glutamic acid," Dental Materials Journal, 34 (5) 707–712 (2015). doi:10.4012/dmj.2015-064.

10) W.N.F.S.W. Dagang, S.H. Marwan, J. Mahmud, N.F.A. Manan, and A.H. Abdullah, "The influence of pore size and material properties on biomechanical analysis of parietal-temporal implant," Evergreen, 8 (4) 750–758 (2021). doi:10.5109/4742118.

11) T. Kokubo, H.M. Kim, and M. Kawashita, "Novel bioactive materials with different mechanical properties," Biomaterials, 24 (13) 2161–2175 (2003). doi:10.1016/S0142-9612(03)00044-9.

12) A.H. Abdullah, and M. Todo, "Effects of total hip arthroplasty on stress adaptation and bone remodeling in lower limbs," Evergreen, 2 (1) 6–11 (2015). doi:10.5109/1500422.

13) D. Zhang, Q. Han, K. Yu, X. Lu, Y. Liu, Z. Lu, and Q. Wang, "Antibacterial activities against porphyromonas gingivalis and biological characteristics of copper-bearing peo coatings on magnesium," Journal of Materials Science and Technology, 61 33–45 (2021). doi:10.1016/j.jmst.2020.05.025.

14) B. Bermúdez-Reyes, A.B. Bermúdez-Reyes, F.J. Espinoza-Beltrán, I. Espitia-Cabrera, and M.E. Contreras-García, "Characterzation of ha/zro2-base

bilayer on 316l stainless steel substrates for orthopedic prosthesis application characterization of ha/zro2-base bilayer on 316l stainless steel substrates for orthopedic prosthesis applications topics covered," **4** (2008). doi:10.2240/azojomo0264.

15) S. Dash, S. Singh, and Sanjay Kumar Singh, "Cytotoxicity of nanoparticles used in cosmetic industries: an in-depth insight," *Evergreen*, **9** (*1*) 93–101 (2022). doi:10.5109/4774220.

16) S.P. Dwivedi, M. Maurya, N.K. Maurya, A.K. Srivastava, S. Sharma, and A. Saxena, "Utilization of groundnut shell as reinforcement in development of aluminum based composite to reduce environment pollution: a review," *Evergreen*, **7** (*1*) 15–25 (2020). doi:10.5109/2740937.

17) Y. Phanny, and M. Todo, "Effect of sintering time on microstructure and mechanical properties of hydroxyapatite porous materials for bone tissue engineering application," *Evergreen*, **1** (*2*) 1–4 (2014). doi:10.5109/1495025.

18) S. Hwang, and M. Todo, "Biomechanical Effect of Implantation of Chitosan/MWNTs Reinforced Scaffold into Damaged Femur," *Evergreen*, **7** (*1*) 1–6 (2013).

19) D. Annur, F. Bayu, S. Supriadi, and B. Suharno, "Electrophoretic Deposition of Hydroxyapatite/Chitosan Coating on Porous Titanium for Orthopedic Application," *Evergreen*, **9** (*1*) 109-114 (2022). doi:105109/4774222.

20) S.B. Goodman, Z. Yao, M. Keeney, and F. Yang, "The future of biologic coatings for orthopaedic implants," *Biomaterials*, **34** (*13*) 3174–3183 (2013). doi:10.1016/j.biomaterials.2013.01.074.

21) M. Fazel, H.R. Salimijazi, M. Shamanian, I. Apachitei, and A.A. Zadpoor, "Influence of hydrothermal treatment on the surface characteristics and electrochemical behavior of ti-6al-4v bio-functionalized through plasma electrolytic oxidation," *Surface and Coatings Technology*, **374** 222–231 (2019). doi:10.1016/j.surfcoat.2019.05.088.

22) G.S. Kaliaraj, B. Muthaiah, K. Alagarsamy, V. Vishwakarma, and A.M.K. Kirubaharan, "Role of bovine serum albumin in the degradation of zirconia and its allotropes coated 316l ss for potential bioimplants," *Materials Chemistry and Physics*, **258** (2021). doi:10.1016/j.matchemphys.2020.123859.

23) G.S. Kaliaraj, V. Vishwakarma, K. Kirubaharan, T. Dharini, D. Ramachandran, and B. Muthaiah, "Corrosion and biocompatibility behaviour of zirconia coating by ebpvd for biomedical applications," *Surface and Coatings Technology*, **334** 336–343 (2018). doi:10.1016/j.surfcoat.2017.11.047.

24) M.I. Alhamid, M.A. Rainanda, and R. Miftah, "Effectiveness analysis of ozonation for prevention of corrosion and precipitation of crust in closed system cooling towers," *Evergreen*, **8** (*4*) 904–909 (2021). doi:10.5109/4742140.

25) M. Mardali, H.R. SalimiJazi, F. Karimzadeh, B. Luthringer, C. Blawert, and S. Labbaf, "Comparative study on microstructure and corrosion behavior of nanostructured hydroxyapatite coatings deposited by high velocity oxygen fuel and flame spraying on az61 magnesium based substrates," *Applied Surface Science*, **465** 614–624 (2019). doi:10.1016/j.apsusc.2018.09.127.

26) R.J. Talib, S. Saad, M.R.M. Toff, and H. Hashim, "THERMAL SPRAY COATING TECHNOLOGY-A REVIEW," 2003.

27) C.D. Prasad, S. Joladarashi, and M.R. Ramesh, "Comparative investigation of HVOF and flame sprayed CoMoCrSi coating," in: AIP Conference Proceedings, American Institute of Physics Inc., 2020. doi:10.1063/5.0003883.

28) S.P. Dwivedi, M. Maurya, and S.S. Chauhan, "Mechanical, physical and thermal behaviour of sic and mgo reinforced aluminium based composite material," *Evergreen*, **8** (*2*) 318–327 (2021). doi:10.5109/4480709.

29) Z. Bergant, and J. Grum, "Porosity evaluation of flame-sprayed and heattreated nickel-based coatings using image analysis," *Image Analysis and Stereology*, **30** (*1*) 53–62 (2011). doi:10.5566/ias.v30.p53-62.

30) A.S. Baskoro, M.A. Amat, R.D. Putra, A. Widyianto, and Y. Abrara, "Investigation of temperature history, porosity and fracture mode on aa1100 using the controlled intermittent wire feeder method," *Evergreen*, **7** (*1*) 86–91 (2020). doi:10.5109/2740953.

31) W. Winarto, N. Sofyan, and D. Rooscote, "Porosity and wear resistance of flame sprayed tungsten carbide coatings," in: AIP Conference Proceedings, American Institute of Physics Inc., 2017. doi:10.1063/1.4985482.

32) J. Pan, S. Hu, L. Yang, K. Ding, and B. Ma, "Numerical analysis of flame and particle behavior in an hvof thermal spray process," *Materials and Design*, **96** 370–376 (2016). doi:10.1016/j.matdes.2016.02.008.

33) T.C. Hanson, and G.S. Settles, "Particle Temperature and Velocity Effects on the Porosity and Oxidation of an HVOF Corrosion-Control Coating," n.d.

34) S. Oh, and S. Jin, "Titanium oxide nanotubes with controlled morphology for enhanced bone growth," *Materials Science and Engineering C*, **26** (*8*) 1301–1306 (2006). doi:10.1016/j.msec.2005.08.014.

35) H. Luo, D. Goberman, L. Shaw, and M. Gell, "Indentation fracture behavior of plasma-sprayed nanostructured Al 2 O 3 Á/ 13wt.%TiO 2 coatings," n.d. www.elsevier.com/locate/msea.

36) H. Miyazaki, I. Ushiroda, D. Itomura, T. Hirashita, N. Adachi, and T. Ota, "Thermal expansion of hydroxyapatite between - 100 °c and 50 °c," *Materials Science and Engineering C*, **29** (*4*) 1463–1466 (2009). doi:10.1016/j.msec.2008.12.001.

37) V.G. Zavodinsky, "The mechanism of ionic conductivity in stabilized cubic zirconia," *Physics of the Solid State*, **46** (*3*) 453–457 (2004). doi:10.1134/1.1687859.

38) D.J. Curran, T.J. Fleming, M.R. Towler, and S. Hampshire, "Mechanical properties of hydroxyapatite-zirconia compacts sintered by two different sintering methods," *Journal of Materials Science: Materials in Medicine*, **21** (*4*) 1109–1120 (2010). doi:10.1007/s10856-009-3974-z.

39) C.R. Raghavendra, S. Basavarajappa, and I. Sogalad, "Adhesive strength and tribological behaviour of ni–nano-al2o3 composite coating," *Indian Journal of Physics*, **95** (*3*) 423–431 (2021). doi:10.1007/s12648-019-01661-x.

40) A. Ostadi, S.H. Hosseini, and M.E. Fordoei, "The effect of temperature and roughness of the substrate surface on the microstructure and adhesion strength of eb-pvd zro2-%8wty2o3 coating," *Ceramics International*, **46** (*2*) 2287–2293 (2020). doi:10.1016/j.ceramint.2019.09.217.

41) A. Wennerberg, and T. Albrektsson, "Suggested Guidelines for the Topographic Evaluation of Implant Surfaces," 2000.

42) D.D. Deligianni, N. Katsala, S. Ladas, D. Sotiropoulou, J. Amedee, and Y.F. Missirlis, "E!ect of surface roughness of the titanium alloy Ti}6Al}4V on human bone marrow cell response and on protein adsorption," 2001.

43) K. Anselme, P. Linez, M. Bigerelle, D. le Maguer, A. le Maguer, P. Hardouin, H.F. Hildebrand, and J.M. Leroy, "The relative in#uence of the topography and chemistry of TiAl6V4 surfaces on osteoblastic cell behaviour," 2000.

44) D.J. Kong, D. Long, Y.Z. Wu, and C.Z. Zhou, "Mechanical properties of hydroxyapatite-zirconia coatings prepared by magnetron sputtering," *Transactions of Nonferrous Metals Society of China (English Edition)*, **22** (*1*) 104–110 (2012). doi:10.1016/S1003-6326(11)61147-3.

45) D.G. Castner, and B.D. Ratner, "Proteins Controlled With Precision at Organic, Polymeric, and Biopolymer Interfaces for Tissue Engineering and Regenerative Medicine," in: Principles of Regenerative Medicine, Elsevier, 2019: pp. 523–534. doi:10.1016/b978-0-12-809880-6.00031-x.

46) H.M. Kim, T. Himeno, M. Kawashita, T. Kokubo, and T. Nakamura, "The mechanism of biomineralization of bone-like apatite on synthetic hydroxyapatite: an in vitro assessment," *Journal of the Royal Society Interface*, **1** (*1*) 17–22 (2004). doi:10.1098/rsif.2004.0003.

47) L. Benea, "Electrodeposition and tribocorrosion behaviour of zro2-ni composite coatings," *Journal of Applied Electrochemistry*, **39** 1671–1681 (2009). doi:10.1007/s10800-009-9859-5.

48) D. Zhang, Y. Ge, G. Liu, F. Gao, and P. Li, "Investigation of tribological properties of micro-arc oxidation ceramic coating on mg alloy under dry sliding condition," *Ceramics International*, **44** (*14*) 16164–16172 (2018). doi:10.1016/j.ceramint.2018.05.137.

49) N. Barth, C. Schilde, and A. Kwade, "Influence of particle size distribution on micromechanical properties of thin nanoparticulate coatings," in: Physics Procedia, Elsevier B.V., 2013: pp. 9–18. doi:10.1016/j.phpro.2012.12.002.

50) Z. Xi, Y. Wu, S. Xiang, C. Sun, Y. Wang, H. Yu, Y. Fu, X. Wang, J. Yan, D. Zhao, Y. Wang, and N. Zhang, "Corrosion resistance and biocompatibility assessment of a biodegradable hydrothermal-coated mg-zn-ca alloy: an in vitro and in vivo study," *ACS Omega*, **5** (*9*) 4548–4557 (2020). doi:10.1021/acsomega.9b03889.

51) S. Hiromoto, and M. Tomozawa, "Hydroxyapatite coating of az31 magnesium alloy by a solution treatment and its corrosion behavior in nacl solution," *Surface and Coatings Technology*, **205** (*19*) 4711–4719 (2011). doi:10.1016/j.surfcoat.2011.04.036.

52) S. Yugeswaran, C.P. Yoganand, A. Kobayashi, K.M. Paraskevopoulos, and B. Subramanian, "Mechanical properties, electrochemical corrosion and in-vitro bioactivity of yttria stabilized zirconia reinforced hydroxyapatite coatings prepared by gas tunnel type plasma spraying," *Journal of the Mechanical Behavior of Biomedical Materials*, **9** 22–33 (2012). doi:10.1016/j.jmbbm.2011.11.002.

53) E. Celik, I. Ozdemir, E. Avci, and Y. Tsunekawa, "Corrosion behaviour of plasma sprayed coatings," *Surface and Coatings Technology*, **193** (*1-3 SPEC. ISS.*) 297–302 (2005). doi:10.1016/j.surfcoat.2004.08.143.

54) K. Sasaki, and G.T. Burstein, "Erosion-corrosion of stainless steel under impingement by a fluid jet," *Corrosion Science*, **49** (*1*) 92–102 (2007). doi:10.1016/j.corsci.2006.05.012.

55) R. Kumari, and J.D. Majumdar, "Studies on corrosion resistance and bio-activity of plasma spray deposited hydroxylapatite (ha) based tio 2 and zro 2 dispersed composite coatings on titanium alloy (ti-6al-4v) and the same after post spray heat treatment," *Applied Surface Science*, **420** 935–943 (2017). doi:10.1016/j.apsusc.2017.05.208.

56) W.W. Davis, and T.R. Stout, "Disc Plate Method of Microbiological Antibiotic Assay I. Factors Influencing Variability and Error1," 1971.

57) M. Sahlan, D.K. Mandala, D.K. Pratami, R. Adawiyah, A. Wijarnako, K. Lischer, and A. Fauzi, "Exploration of the antifungal potential of indonesian propolis from tetragonula biroi bee on candida sp. and cryptococcus neoformans," *Evergreen*, **7** (*1*) 118–125 (2020). doi:10.5109/2740968.